Front. Earth Sci. 2021, 15(2): 438–456
https://doi.org/10.1007/s11707-021-0915-8

RESEARCH ARTICLE

Differences in hydrocarbon composition of shale oils in different phase states from the Qingshankou Formation, Songliao Basin, as determined from fluorescence experiments

Longhui BAI[1], Bo LIU (✉)[2,1], Jianguo YANG[3], Shansi TIAN[1], Boyang WANG[1], Saipeng HUANG[1]

1 Accumulation and Development of Unconventional Oil and Gas, State Key Laboratory Cultivation Base, Northeast Petroleum University, Daqing 163318, China
2 Hubei Key Laboratory of Petroleum Geochemistry and Environment, Yangtze University, Wuhan 430100, China
3 Shenyang Center, China Geological Survey, Shenyang 110034, China

Abstract The phase state of shale oil has a significant impact on its mobility. The mineral and organic matter in shale reservoirs play an important role in oil phase. This study attempts to evaluate the properties of shale oils in different phase states and to investigate how these differences are related to initial shale composition. Samples from the first member of the Qingshankou (Q1) Formation were analyzed using X-ray diffraction, total organic carbon content, rock pyrolysis solvent extraction and group component separation. Subsequently, fluorescence techniques were used to quantitatively determine the content and properties of the free oil (FO), the adsorbed oil associated with carbonate (ACO), and the adsorbed oil associated with silicate and clay-organic complexes (AKO). The results showed that non-hydrocarbons and asphaltenes are the primary fluorescing compounds on shale grain. FO is the dominant phase in the Q1 Formation. The quantitative grain fluorescence on extraction (QGF-E) and total scanning fluorescence (TSF) spectra of ACO and AKO show a significant redshift compared to the FO. The TSF spectra of FO have a characteristic skew to the left and a single peak distribution, suggesting a relatively light hydrocarbon component. The TSF spectra of ACO show a skew to the right and an even, double-peaked distribution. The TSF spectra of AKO show a single peak with a skew to the right, indicating that ACO and AKO hydrocarbons are heavier than FO hydrocarbons. In summary, enrichment of carbonate minerals in shale may result in misidentification of "sweet spots" when using QGF. The normalized fluorescence intensity of QGF-E and TSF are effective indexes allowing oil content evaluation. As an additional complicating factor, hydrocarbon fractionation occurs during generation and expulsion, leading to a differentiation of oil composition. And FO has high relatively light hydrocarbon content and the strongest fluidity.

Keywords stepwise extraction, fluorescence spectroscopic techniques, shale grain, shale oil phase

1 Introduction

In recent years, organic-rich shales have been considered a prospective target in the development of unconventional oil and gas resources, and an important supplement to adjacent depleted conventional oil and gas resources (Jarvie et al., 2007; Zou et al., 2010; Rivard et al., 2014). This has been confirmed over recent decades from the extensive development of marine shale oil and gas resources in North America, and China has also recently increased its unconventional oil and gas resource exploration and development efforts (Curtis, 2002; Zou et al., 2010; Hou et al., 2017; Liu et al., 2019a; Liu et al., 2020; Gong et al., 2021; Zeng et al., 2021.) The first member of Qingshankou (Q1) Formation in Songliao Basin is a typical continental shale oil-bearing stratum in China. In 2018, the Guye Youping 1 well deployed in Gulong Sag, northern Songliao Basin, achieved a high-yielding industrial oil flow of 30.5 t/d in the Q1 Formation, showing a broad prospect for continental shale oil development (Sun et al., 2021).

Oil phase state plays a significant role in oil production,

Received January 16, 2021; accepted June 3, 2021

E-mail: liubo@nepu.edu.cn

retention and transfusion, and it also has an important influence on production methods selection (Jarvie et al., 2007; Li et al., 2018; Zhang et al., 2019). Oil can be subdivided into free and adsorbed states, either stored in pore spaces within shale reservoirs or on mineral and kerogen surfaces (Loucks et al., 2012; Jiang et al., 2016; Romero-Sarmiento, 2019). The inorganic minerals in continental shales mainly consists of quartz, feldspar, carbonates and clays. Intergranular pores and intragranular pores are the primary accumulation spaces for free oil. Mineral grain provides adsorption surfaces for adsorbed oil (Liu and Eadington, 2005). Additionally, organic matter (OM), an important component of shale, can provide considerable pore space for the accumulation of free oil under certain maturity related conditions. The "kerogen network" formed by kerogen particles pervasively distributed through the shale can also provide a large number of adsorption surfaces for oil (Liu et al., 2019, 2021). During the shale thermal evolution process, OM and its derived products interact with inorganic minerals for example: (a) the dissolution of carbonate minerals by organic acids produced in the process of hydrocarbon generation (Loucks et al., 2012), and (b) the role clay minerals play in promoting mature OM hydrocarbon generation (Spiro, 1978).

Several experimental methods allow the quantitative sub-division of shale oil into different phase states. These include multi-step pyrolysis (Romero-Sarmiento et al., 2015; Li et al., 2018, 2019; Li et al., 2020), two-dimensional (2D) NMR (Fleury and Romero-Sarmiento., 2016; Liu et al., 2019b) and stepwise extraction (Spiro,1984; Pan et al., 2019; Zhang et al., 2019). During multi-step pyrolysis, a powdered shale sample undergoes thermal desorption at a set heating rate. The hydrocarbons released at different temperature intervals are detected using a Gas Chromatography-Mass Spectrometer (GC-MS) to determine the temperature intervals corresponding to different oil phase states, including the free state, the adsorbed state and cracked hydrocarbons derived from kerogen. According to earlier studies (Romero-Sarmiento et al., 2015; Jiang et al., 2016; Li et al., 2018), free oil, primarily composed of relatively light hydrocarbons (saturated and aromatic hydrocarbons with lower carbon number), are desorbed at temperatures below 200°C. This means that this temperature is an important factor in the identification of shale reservoir "sweet spots." Different oil phase states within shale reservoirs have different longitudinal (T_1) and transverse (T_2) relaxation times. The magnitude of the T_1/T_2 value reflects the viscosity of the ^{1}H-rich material (kerogen, asphaltene, water, hydrocarbons, etc.) in the porous medium. The higher the T_1/T_2 value, the higher the viscosity of the fluid (Liu et al., 2019a). Therefore, the 2D NMR method can be used to quantify the spatial distribution of oil in different phase states. These two methods however focus on the quantitative measurement of free oil content; the influence of shale mineralogy and OM composition on oil phase are ignored. Additionally, these two methods cannot separate and extract oil in different phase states from shale reservoirs. Compared with multi-step pyrolysis and two-dimensional NMR, the stepwise extraction method provides a way to separate and extract bitumen in different phase states. By dissolving the shale sample, bitumen in different phase states can be extracted in a sequence that is related to their spatial and geochemical relationship with minerals and OM in the samples (Spiro, 1984; Guan et al., 1998; Pan et al., 2018; Pan et al., 2019).

OM maturity is known to have an impact on the composition of bitumen in different phase states (Spiro, 1978, 1984). The results of GC-MS analysis of samples from marine shales of different maturities show that the biomarker distribution of bitumen in different phase states from low maturity shales is primarily related to the OM and mineral sedimentary sources. With increasing maturity, clay minerals form hydrogen bonds with OM, and the biomarkers of bitumen in different phase states differ significantly. For example, isoalkanes and alkylcyclohexanes are only found in the adsorbed bitumen (Spiro, 1978). This artificial thermal desorption experiment was carried out on type II organic-rich shales, and shale samples with different maturities were obtained. The bitumen in different phase states, extracted from shales of different maturities, were obtained by stepwise extraction, and negative-ion electrospray (ESI), and Fourier Transform Ion Cyclotron Resonance Mass Spectrometry (FT-ICR MS) were then used to analyze the oil samples (Pan et al., 2019). The results show the difference in composition of bitumen in the different phase states. For example, neutral nitrogen compounds only exist in the free oil (FO), while acidic compounds are principally found in the adsorbed oil. With increasing OM maturity, the content of acidic components decreases in both free and adsorbed oil samples, as the process of hydrocarbon expulsion also leads to differential enrichment of acidic components. In general, the original mineral composition and OM characteristics of a shale have a significant impact on the composition of shale oils in different phase states.

Although the properties and components of bitumen in different phase states can be accurately analyzed using GC-MS or FT-ICR MS, both the methods are labor intensive and costly. Aromatics and polar compounds will produce a characteristic fluorescence when excited by light of appropriate wavelength. Therefore, the compositions and properties of an oil can be derived from the characteristics of its fluorescence spectrum (Stasiuk and Snowdon, 1997; Liu and Eadington, 2005; Liu et al., 2014b). In recent years, fluorescence spectroscopic techniques have been widely used to detect trace hydrocarbons. This has allowed the identification of oil, gas or water layers, ancient oil reservoirs, oil and gas migration paths, and the determination of the properties and the abundance of hydrocarbon inclusions (Liu and Eadington, 2005; Liu et al., 2014b).

The fluorescence spectroscopic techniques include several methods for specific hydrocarbon targets (Liu et al., 2003, 2007). The quantitative fluorescence technology (QGF) targets the hydrocarbons on reservoir grain or in hydrocarbon inclusions, while both the quantitative fluorescence on extraction (QGF-E) and Total Scanning Fluorescence (TSF) experimental methods measure the composition of the free oils, the adsorbed hydrocarbons and the hydrocarbons in inclusions. The advantages of these technologies include the small amount of sample needed, high sensitivity, economy, and the rapid generation of quantitative results. In 2019, Liu combined the QGF-E, TSF and 2D NMR techniques to quantitatively study the oil content and properties of the Q1 Formation in the southern Songliao Basin, China. The shale oil content and properties were confirmed (Liu et al., 2019b). However, the application of the fluorescence spectroscopic techniques was limited to the analysis of free oil and the identification of "sweet spots" in shale reservoirs. The shale grain and the properties of the shale oils in different phase states have not until now been studied using fluorescence spectroscopic techniques.

The following workflow was designed and implemented in order to rapidly and accurately investigate the composition of shale oil in different phase states, and the influence of mineral composition, and the processes of hydrocarbon generation and expulsion on final hydrocarbon compound compositions. Shale samples from the Q1 Formation in the south of the Songliao Basin were selected. The mineral composition and OM characteristics of the shale samples were determined from X-ray diffraction (XRD), TOC analysis, Rock-Eval pyrolysis, soluble OM extraction and group component separation measurements. Subsequently, the fluorescence characteristics of the shale grain and the shale oils in different phase states obtained by stepwise extraction were determined using fluorescence spectroscopy techniques. This allowed the determination and discussion of the content, composition, and properties of shale oils in different phase states.

2 Geological setting

The continental shale samples used in this study were all taken from Well J in the Q1 Formation in the south of the Songliao Basin, northeastern China. The basin's structural divisions are shown in Figs. 1(a). The Songliao Basin is famous for its oil and gas fields. The Q1 Formation is the main source rock in the study area, and is primarily composed of dark continental shales with thin, interbedded

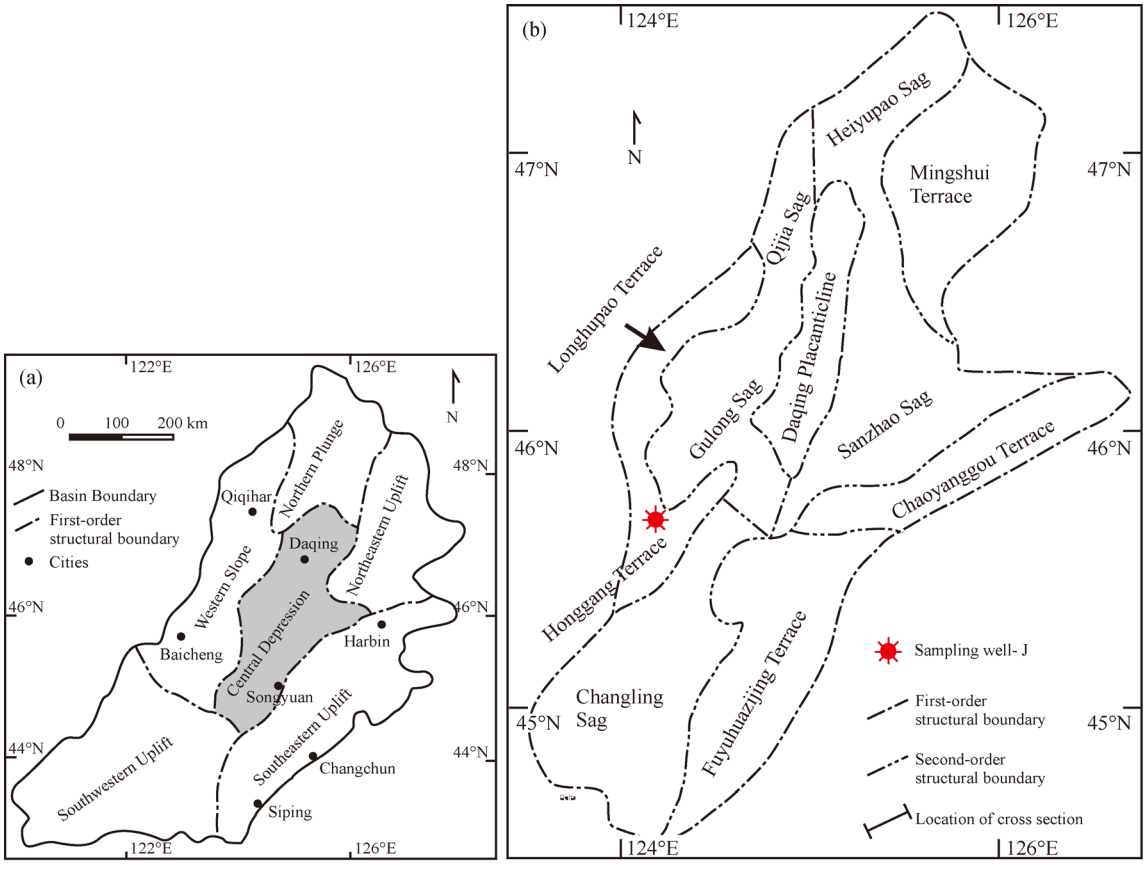

Fig. 1 (a) Tectonic unit division, (b) studied area and location of Well J. (Modified from Liu et al., 2019a).

sand layers. The shales of the Q1 Formation have high OM concentrations, the average TOC is higher than 2.0 wt%. The OM is primarily derived from aquatic organisms, resulting in mostly type I kerogen. R_o values range from 0.5% to 1.1%, and T_{max} values range from 430°C to 450°C, indicating that the maturity of the OM is within the oil generation window. See Liu et al. (2017) for more details on the regional geology. In summary, the Q1 Formation is primarily composed of mature, oil-prone source rocks, which makes it one of the main target formations for shale oil development in China (Zou et al., 2010; Liu et al., 2017; Liu et al., 2019a). The location of sample well J is shown in Fig. 1(b).

3 Samples and experimental methods

A total of 14 shale samples were selected from the Q1 Formation, with sample depth ranging from 1971.18 m to 2062.55 m. TOC measurements, Rock-Eval pyrolysis and XRD analysis were performed on all the samples. Based on mineral composition and OM characteristics, seven representative samples were selected for organic geochemical analysis, and column chromatography was used to separate extractable organic matter (EOM) to acquire saturated hydrocarbons, aromatic hydrocarbons, non-hydrocarbons and asphaltenes. Subsequently, stepwise extraction and fluorescence spectroscopic techniques were performed on the remaining samples. All experiments were conducted at the Key Laboratory of "Continental Shale Hydrocarbon Accumulation and Efficient Development (Northeast Petroleum University), Ministry of Education". The flow chart for the whole experimental procedures undertaken as part of this study are shown in Fig. 2.

In this study, a CS-230 analyzer and a Rock-Eval 6 instrument was used to determine the OM characteristics of the shale samples, resulting in a suite of measurements including TOC, S_1, S_2, and T_{max}. Pyrolysis is a widely used and effective way to evaluate source rock both qualitatively and quantitatively. The increasing importance of unconventional oil and gas resources has led to a rise in the application of this technique. Free oil is the primary economic resource in unconventional reservoirs, and measurement of S_1 gives an indication of the amount of free oil in the shale reservoir. This value S_1, along with its ratio to TOC is considered to be one of the important indicators of whether a shale oil reservoir is economic (Jarvie, 2012; Li et al., 2016; Liu et al., 2019b; Liu and Ostadhassan., 2019). A D8AA25 X-ray diffractometer, made by Bruker, Germany, was used for mineralogical analysis, and the content of quartz, feldspar, carbonate, and clay minerals were determined. As measured diffraction peak intensity does not follow a simple linear relationship with mineral content, X-ray diffraction measurements should only be considered to be semiquantitative (Guo et al., 2018; Gao et al., 2020; Li et al., 2020a).

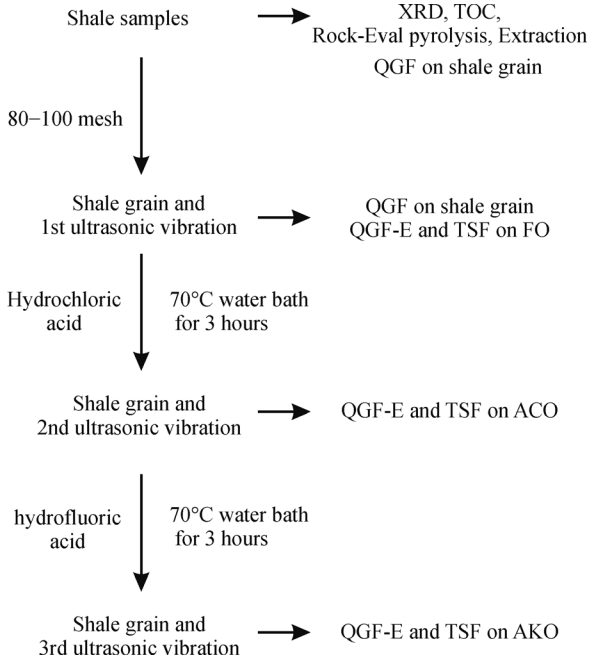

Fig. 2 Flow chart of the whole experimental procedure.

A Soxhlet extraction apparatus was used to determine the EOM content of 7 representative shale samples. The soluble OM in shale was extracted using polar organic solvent at 70°C for 3 days. Column chromatography was then used to separate the individual molecular components of the EOM. Following removal of asphaltenes using n-pentane, different polar organic solvents were washed through the silica gel alumina chromatography column, and saturated hydrocarbons, aromatic hydrocarbons, non-hydrocarbons and asphaltenes were collected. By contrast to S_1 values obtained via pyrolysis, EOM results represent not only the content of relatively light hydrocarbons in shale oils, but also the non-hydrocarbons and asphaltenes. Consequently, these results more closely indicate the real shale oil composition and are more representative of the shale oil content of the reservoir (Liu et al., 2014b).

The Cary Eclipse Fluorescence Spectrophotometer produced by Agilent was used to conduct fluorescence experiments on solid shale grain and oils in different phase states. These experiments showed that ultraviolet light with excitation wavelengths of 254 nm and 228 nm were optimal for the investigation of clastic rock samples and carbonate rock reservoir samples, respectively. These wavelengths maximized the detection of hydrocarbon compounds adsorbed onto grain (Liu et al., 2007; Liu et al., 2009; Liu et al., 2014b). After all the samples were subjected to light at 254 nm, an excitation wavelength of 228 nm was applied to detect shale grain rich in carbonate minerals. It should be noted that the theory that measured fluorescence intensity shows a positive correlation with oil

concentration in solution assumes that no fluorescence quenching occurs (Liu and Eadington, 2005). Fluorescence quenching refers to the phenomenon whereby fluorescence intensity decreases abnormally. The fluorescence time shortens following irradiation due to the presence of a quenching agent or high concentrations of the fluorescing substance. This means that during fluorescence experiments investigating oils in different phase states, the investigator must ensure that oil concentration does not exceed the detection limit (Liu and Eadington, 2005). Similarly, in order to optimize the detection of different hydrocarbon compounds, the QGF-E detection was set at an excitation wavelength of 260 nm, and emitted wavelengths between 300 and 600 nm were recorded. TSF detection was set to synchronous scanning mode in order to record emission fluorescence wavelengths generated by excitation wavelengths of 220–340 nm.

The stepwise extraction combined with fluorescence investigation workflow is summarized as follows: first, shale samples were selected and ground to 80–100 mesh, and QGF was performed on the solid shale grain. Then the sample grain was recovered, and 20 mL of dichloromethane (DCM) was added to 2 g of shale sample. This solution was subjected to three ultrasonic vibration intervals lasting 20 min, each vibration interval followed by a 10 min 'relaxation' interval. Subsequently the supernatant was sampled to obtain FO. To ensure complete sampling of FO and avoid sampling hydrocarbons related to carbonate minerals, this vibration process was repeated until the fluorescence intensity of the supernatant was negligible. QGF was than performed on the shale grain following removal of FO to evaluate the residual adsorbed hydrocarbons on shale grain. Then 20% hydrochloric acid solution was added to the remaining shale grain, and, and the resulting mixture was heated at 70°C in a water bath for 3 h until the carbonate minerals were completely dissolved. The remaining solution was rinsed with ultra-pure water to neutralize it and the sample grain were recovered following drying at 70°C. As in the FO extraction above, following the addition of 20 mL of dichloromethane (DCM) a further series of ultrasonic vibration intervals was performed on the remaining sample grain to obtain ACO. Finally, hydrofluoric acid solution was added to 7 representative samples. These samples were then heated in a 70°C water bath for 3 h until quartz and other minerals were completely dissolved, and the clay-organic components were extracted. The resulting material was dried at 70°C and the same ultrasonic vibration method was used to obtain AKO. QGF-E and TSF were subsequently applied to the extracted FO, ACO, and AKO samples. It should be noted that the DCM and other solutions used in the experiments were non-fluorescent or had fluorescence intensities of < 5 photometer counts (pc). This ensured that there would be no impact on the fluorescence measurements. To minimize evaporation due to the high volatility of DCM, DCM solution was kept at –4°C during these experiments. The final experimental results were normalized to 1 g sample grain and 20 mL of DCM liquid. The parameters QGF intensity, QGF Max and λ_{max} were derived from the QGF experiments. The parameters TSF Max, Max Ex, Max Em, and R_1 were derived from the TSF experiments. QGF intensity and TSG Max values can be considered to represent reservoir oil content, and λ_{max}, Max Ex, Max Em, and R_1 represent the oil quality (Liu et al., 2009; Liu et al., 2014b).

And it should be noted that in this study, the bitumen obtained using different extraction approaches was defined as a shale oil in a different phase state. Absorbed bitumen associated with silicate and clay-organic complexes (AKO) may also contain soluble solid bitumen.

4 Results

4.1 The Q1 Formation shale composition

4.1.1 Organic matter characteristics

The results of the Rock-Eval pyrolysis and TOC experiments are shown in Table 1. The TOC values of shale samples range from 0.34 wt% to 2.68 wt%, with an average value of 1.6 wt%. S_1 values range from 0.2 mg/g to 3.4 mg/g, with an average value of 1.8 mg/g. S_2 values range from 1.7 mg/g to 13.4 mg/g, with an average value of 8.4 mg/g. HI values range from 405 mg/g to 693 mg/g. T_{max} values range from 435°C to 456°C, indicating that the OM is in a mature stage and has generated a large amount of hydrocarbons. As show in Fig. 3(a), the classification of OM type by cross-plotting HI against T_{max}, indicates that the kerogen of the Q1 Formation is predominately Type I and IIa (Espitalié J et al., 1984). A positive correlation between TOC and S_2 was observed with a relatively high coefficient of determination (R^2 = 0.84) (Fig. 3(b)), indicating that the Q1 Formation was deposited in a moderately deep, tectonically stable environment with a continuous sedimentary supply (Langford and Blanc-Valleron, 1990). The kerogen type is observed to be highly homogenous, which is consistent with the results from another well in the nearby study area (Liu et al., 2019b). A reasonable positive correlation was found between TOC and S_1 (Fig. 3(c)), reflecting the role of kerogen as the source material. S_1 is shown to be > 1.0 mg/g for TOC > 1.5 wt%, this differs slightly from results obtained during the above-mentioned study where $S_1 > 1.0$ mg/g was observed when TOC > 2.0 wt%, (Liu et al., 2019b). The suggested reason for this difference is that the depth of the Q1 Formation in this study is deeper, leading to higher OM maturity. Therefore, shales with the same OM content contain a larger proportion of lighter-hydrocarbons. The relationship between TOC and S_1 from sample J13 is outside the overall trend (Fig. 3(c)). The S_1 value of this sample, which indicates a relatively light hydrocarbon

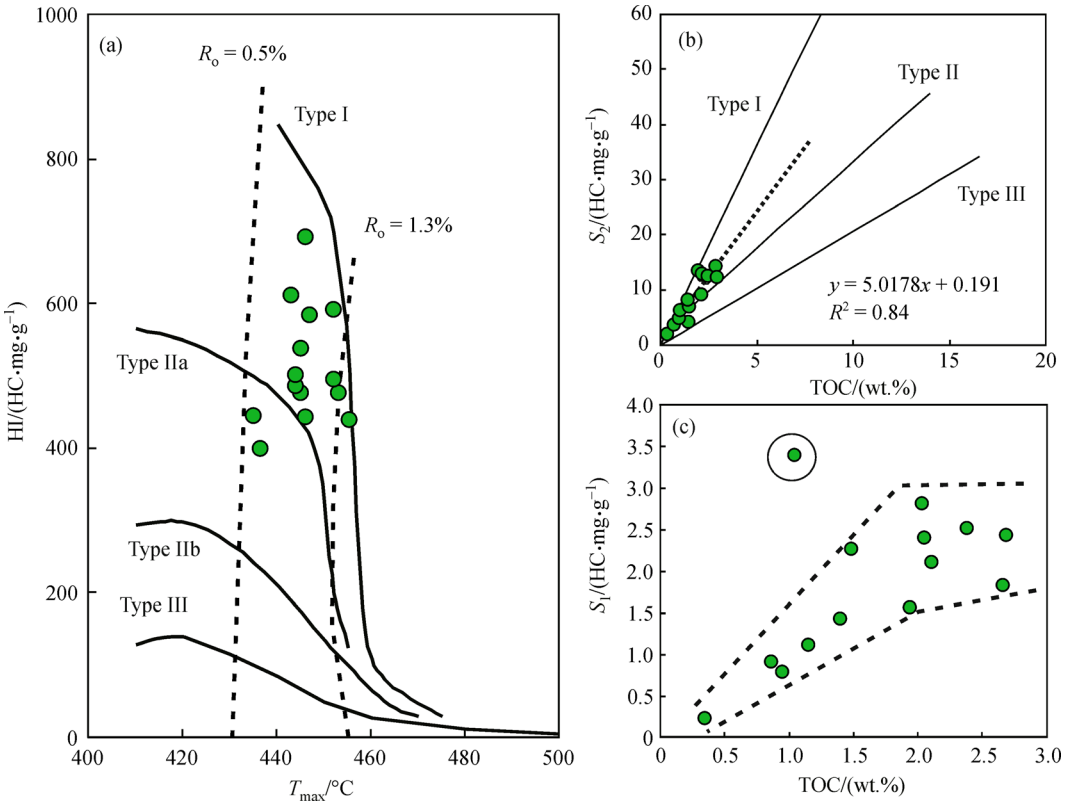

Fig. 3 (a) Plot of T_{max} versus HI. (b) Correlation between S_2 and TOC. (c) Plot of S_1 and TOC.

content, is significantly higher than that recorded in the other samples. It is theorized that this observed discrepancy may be due to the injection of exogenous light hydrocarbons from an adjacent layer.

4.1.2 Mineral composition

The XRD results are shown in Table 1. The mineral composition of the continental shales of the Q1 Formation is strongly heterogenous (Fig. 4(a)). The quartz content of the shale samples ranges from 1.90% to 41.0% (with an average content of 26.4%). The clay content ranges from 4.0% to 41.1% (with an average content of 29.0%). The plagioclase content ranges from 1.8% to 26.8% (with an average content of 15.6%). Only samples J9 and J12 contain K-feldspar (3.4% and 1.6%, respectively). Calcite and ankerite are the main carbonate minerals detected. The calcite content ranges from 0 to 66.1% (with an average content of 8.8%). and the ankerite content ranges from 0 to 92.3% (with an average content of 16.5%). Siderite and pyrite are commonly observed in all the shale samples. The content of siderite in most samples is greater than 3.0%, with an average content of 3.69%. The content of pyrite ranges from 0.4% to 9.5%. It should be noted that the J3, J5, and J13 sample mineralogies are primarily carbonates. Samples J3 and J5 are composed of ankerite, (92.3% and 86.0%, respectively). The mineral composition of sample J13 is primarily calcite, with a content of 66.1%.

Clay minerals identified were mainly illites and mixed layer illite/smectites. Montmorillonite and kaolinite were not detected although a small amount of chlorite was noted. These results indicate that the rock is in the mesodiagenesis stage A–B (Morad et al., 2000). Illite content ranges from 50% to 93% with an average content of 75%. The content of mixed layer illite/smectite ranges from 6% to 27%, with an average content of 16%. Chlorite content ranges from 1% to 23%, with an average content of 8%. The overall composition characteristics of the clay minerals are shown in Fig. 4(b).

4.1.3 Soluble organic matter and group composition

The results of the soluble OM extraction and the group compounds of the EOM from 7 representative samples are shown in Table 2. The EOM content ranges from 0.24 wt% to 0.89 wt%, with an average content of 0.58 wt%. Saturated hydrocarbon content ranges from 51.3 wt% to 62.4 wt%, with an average content of 58.4 wt% and is the main component of the group compounds. The second most abundant component is aromatic hydrocarbon, and the content ranges from 14.4 wt% to 18.9 wt%, with an average content of 17.0 wt%. The content of non-hydrocarbons and asphaltenes is lower, the content of non-hydrocarbon ranges from 7.5 wt% to 14.6 wt%, with

Table 1 Bulk geochemical parameters and XRD results of the shale samples of the Q1 Formation

Number	Depth/m	Rock-Eval.						Whole Rock Mineralogy/%								Clay (Phyllosilicate) Mineralogy /%		
		TOC/wt.%	T_{max}/°C	S_1/(mg ·HC·g^{-1})	S_2/(mg ·HC·g^{-1})	OSI/(mg ·HC·g^{-1})	HI/(mg HC·g^{-1} TOC^{-1})	Quartz	K-feldspar	Plagioclase	Calcite	Ankerite	Siderite	Pyrite	Total Clay	Illite	chlorite	Illite/ Smectite
J1	1971.18	1.94	446	1.6	13.4	37.0	693	27.7	0	18.0	9.7	0	3.3	5.5	35.8	74	7	19
J2	1976.86	1.40	447	1.4	8.2	29.4	584	32.9	0	17.0	3.1	4.4	2.1	5.2	35.3	85	2	13
J3	1985.73	0.34	444	0.2	1.7	57.6	487	1.9	0	1.8	0	92.3	0	0	4.0	66	12	22
J4	1987.62	0.86	445	0.9	4.6	47.5	539	34.4	0	19.3	0.4	0	0	5.1	40.8	93	1	6
J5	1989.67	0.95	444	0.8	4.8	41.3	502	4.9	0	2.3	0	86.0	0	0	6.8	50	23	27
J6	2003.73	2.66	453	1.8	12.7	55.7	476	23.6	0	23.5	0.3	20.7	0	3.1	28.8	61	12	27
J7	2009.67	1.48	445	2.3	7.1	53.6	478	26.9	0	25.3	2.7	16.5	1.2	4.1	23.3	75	8	17
J8	2020.90	1.15	436	1.2	4.7	41.7	405	34.0	0	18.6	3.7	0	0	3.1	40.6	89	2	9
J9	2025.45	2.05	446	2.4	9.1	37.1	444	30.0	3.4	26.8	7.3	0	1.1	3.0	28.4	72	10	18
J10	2035.55	2.03	435	2.8	9.1	57.0	446	30.0	0	14.2	10.9	5.8	0	1.7	37.5	74	9	17
J11	2048.18	2.11	452	2.1	12.5	71.9	593	35.0	0	12.4	9.6	0	0	1.9	41.1	87	4	9
J12	2051.29	2.38	452	2.5	11.8	43.6	496	33.5	1.6	18.5	4.5	0	0	3.6	38.2	76	8	16
J13	2055.60	1.04	443	3.4	6.4	29.2	612	14.0	0	8.0	66.1	5.0	0.4	2.1	4.3	84	4	12
J14	2062.55	2.68	456	2.3	11.5	45.6	430	41.0	0	12.9	4.5	0	0	0.6	41.0	68	16	16

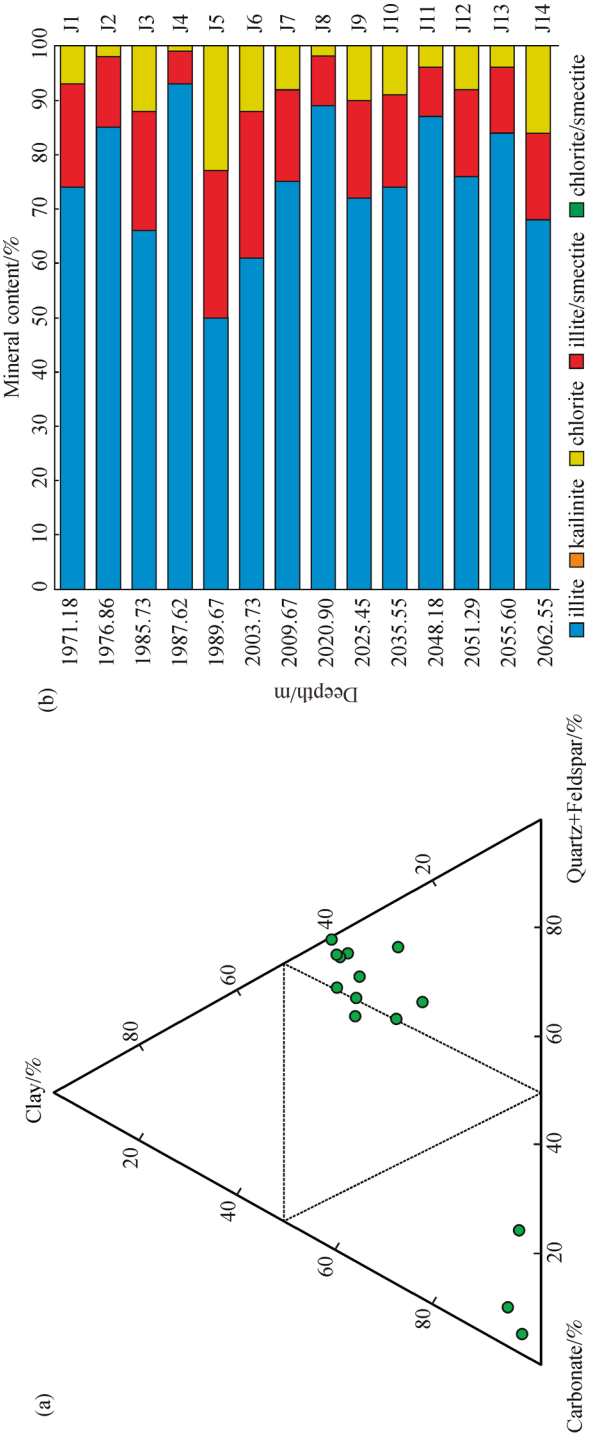

Fig. 4 (a) Triangular plot of rock mineral composition of the Q1 Formation. (b) Bar graph of clay mineral content of the Q1 Formation.

an average content of 10.5 wt.%, and the content of asphaltene ranges from 4.4 wt.% to 17.7 wt.%, with an average content of 8.6 wt.%. The soluble OM in the Q1 Formation is primarily composed of saturated and aromatic hydrocarbons (Fig. 5).

4.2 Results of stepwise extraction and fluorescence investigations

4.2.1 QGF of continental shale grain

The QGF results from the shale grain following FO extraction are shown in Table 3. The QGF spectra of the shale sample grain under an excitation wavelength of 254 nm show spectral peaks λ_{max} at around 370 nm with QGF intensities less than 50 pc (Fig. 6(a)). The fluorescence intensities of carbonate-rich samples J3, J5, and J13 are relatively high, the QGF MAX of sample J13 reached 241.3 pc. Whereas the λ_{max} of most of the shale samples are concentrated at around 370 nm, the characteristic peaks in the fluorescence spectra of the J3 and J5 samples are red-shifted with λ_{max} observed at 502.8 nm and 384.1 nm, respectively. The QGF ratio, QGF index, and other measured parameters from the carbonate-rich sample were all higher than those obtained from the shale samples. Figure 6(b) shows the results of using an excitation wavelength of 228 nm on the carbonate-rich samples. In the fluorescence spectra of the carbonate-rich samples measured at 228 nm incident excitation wavelength (Fig. 6(b)), the spectrum peaks λ_{max} of J3-2, J5-2, and J13-2 are 507.2 nm, 367.5 nm, and 371.5 nm, respectively. The QGF MAX and QGF intensities from samples J3-2 and J5-2 show little variation compared to the results derived using an excitation wavelength (EW) of 254 nm. The QGF ratio was reduced from 2.1:1.4 (254 nm EW) to 1.1:0.8 (228 nm EW) and the QGF index was reduced from 26.6:14.7 (254 nm EW) to 3.2:2.0 (228 nm EW). The QGF intensity of J13-2 derived using an excitation wavelength of 254 nm was 143.3 pc, while using an excitation wavelength of 228 nm the recorded value was 450.0 pc.

Following FO extraction, the measured QGF parameters from all the samples changed significantly (Table 3). QGF intensity and QGF MAX, which indicate total hydrocarbon content obviously decreased. Furthermore, when compared with the other samples, the QGF intensities of the

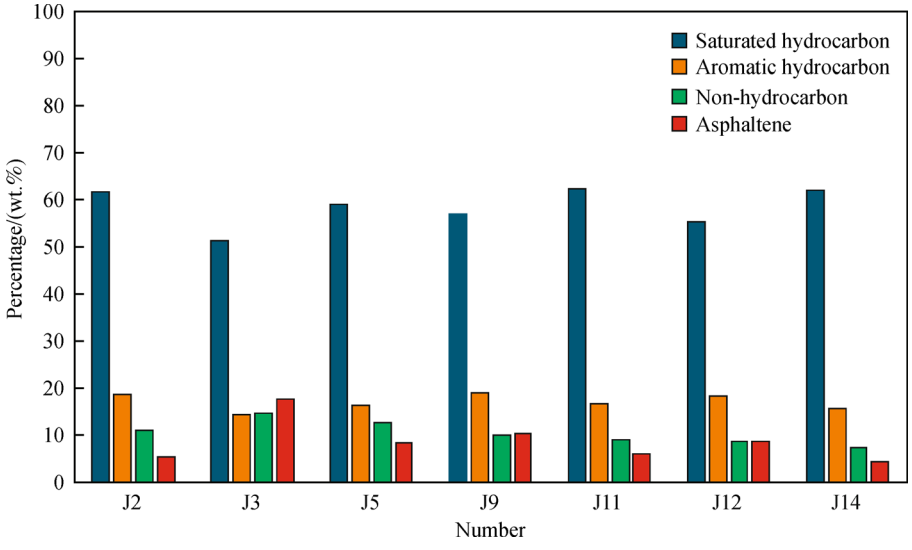

Fig. 5 Percentage content of group components of EOM.

Table 2 Group compounds separation results of the shale samples of the Q1 Formation

Number	Chloroform asphalt "A"/wt.%	Saturated hydrocarbon/%	Aromatic hydrocarbon/%	Non-hydrocarbon /%	Asphaltene/%
J2	0.56	61.8	18.6	11.1	5.3
J3	0.11	51.3	14.4	14.6	17.7
J5	0.24	58.9	16.2	12.7	8.2
J9	0.77	57.1	18.9	10.0	10.2
J11	0.89	62.4	16.8	9.0	5.9
J12	0.85	55.5	18.3	8.7	8.5
J14	0.66	61.9	15.7	7.5	4.4

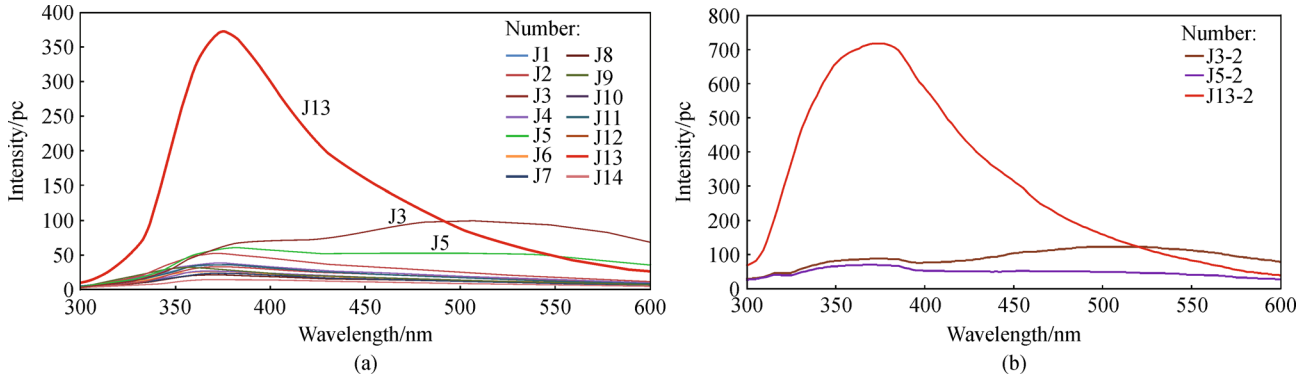

Fig. 6 QGF spectrum of the shale grains of the Q1 Formation.

Table 3 QGF results of the continental shale grains of the Q1 Formation.

Number	Original					Extracted				
	QGF intensity/pc	QGF ratio	QGF index	QGF max/pc	λ_{max}/nm	QGF intensity/pc	QGF ratio	QGF index	QGF Max/pc	λ_{max}/nm
J1	26.5	0.9	5.1	36.0	372.4	9.9	0.7	2.7	14.8	354.1
J2	38.5	0.9	7.8	52.5	373.6	11.2	0.6	2.9	20.4	347.9
J3	83.8	2.1	26.6	106.8	502.8	68.5	2.6	27.1	98.1	517.6
J4	27.9	0.9	5.5	37.9	373.6	11.1	0.6	2.7	18.1	351.1
J5	61.4	1.4	14.7	67.7	384.1	16.5	1.4	8.9	22.6	528.8
J6	16.3	0.9	6.1	21.3	373.2	7.4	0.7	3.4	10.9	353.5
J7	19.4	0.8	7.7	26.2	368.1	9.2	0.5	3.2	19.6	346.3
J8	20.0	0.9	6.2	27.1	371.6	9.1	0.7	3.3	14.0	354.5
J9	19.8	0.6	5.3	32.4	357.4	20.0	0.3	2.5	62.6	346.7
J10	25.7	1.0	7.6	33.4	374.9	10.0	0.9	3.4	12.1	364.3
J11	26.6	0.9	4.8	36.7	374.4	11.1	1.0	3.2	12.5	388.4
J12	17.6	0.9	5.0	23.7	372.9	9.5	0.8	3.2	11.5	358.7
J13	143.3	0.8	16.7	241.3	374.4	31.3	1.0	7.7	36.5	374.1
J14	12.1	1.0	4.7	14.9	376.2	4.8	1.0	3.1	5.5	383.7
J3-2	90.9	1.1	3.2	124.8	507.2	39.8	1.3	3.1	61.5	510.4
J5-2	53.1	0.8	2.0	70.5	367.5	16.4	0.7	1.1	24.7	492.0
J13-2	450.0	0.7	6.5	719.6	371.5	33.5	0.7	1.4	50.4	361.9

carbonate-rich samples were measured at 68.5 pc (J3), 16.5 pc (J5), and 31.3 pc (J13), and the QGF Max reached 98.1 pc (J3), 22.6 pc (J5), and 36.5 pc (J13). The λ_{max} of samples J3 and J5 reached 517.6 nm and 528.8 nm, respectively. The fluorescence spectra of samples J3 and J5 still showed a significant redshift when compared to the fluorescence spectrum from the shale samples.

4.2.2 QGF-E of shale oils in different phase states

The QGF-E and TSF results from shale oils in different phase states are shown in Table 4. The normalized FO QGF-E intensity ranges from 9893.6 pc to 70466.4 pc. As shown in Fig. 7(a), the FO fluorescence spectrum peaks λ_{max} range from 375 nm to 381 nm. The normalized ACO QGF-E intensity ranges from 454.8 pc to 2037 pc. As shown in Fig. 7(b), the ACO fluorescence spectrum peaks λ_{max} range from 362 nm to 389 nm, while the fluorescence spectra peaks λ_{max} of J5 and J8 are 439 nm and 444 nm, respectively. The fluorescence spectra of J5 and J8 show an obvious red-shift. The normalized FO QGF-E intensity ranges from 545.6 pc to 3305.6 pc, all the normalized QGF-E intensity values from the carbonate-rich samples J3 and J5 are lower than 1000 pc. As shown in Fig. 7(c), the spectrum peaks λ_{max} of AKO range from 410 nm to 430 nm, showing significant redshift when compared with the FO spectrum peaks.

Table 4 QGF-E and TSF results of shale oils in different phase states

Number	FO							ACO							AKO						
	QGF-E /pc	λ_{max} /nm	TSF Max /pc	Max Ex /nm	Max Em /nm	R_1	R_2	QGF-E /pc	λ_{max} /nm	TSF Max /pc	Max Ex /nm	Max Em /nm	R_1	R_2	QGF-E /pc	λ_{max} /nm	TSF Max /pc	Max Ex /nm	Max Em /nm	R_1	R_2
J1	45150.4	379	75880.1	258	378	2.984	4.441	748.8	362	1370.5	220	420	2.337	3.303	/	/	/	/	/	/	/
J2	46256.8	376	75754.7	258	378	2.836	4.286	525.8	372	467.6	254	369	1.835	2.803	/	/	/	/	/	/	/
J3	9893.6	381	17722.7	258	378	2.425	3.243	933.5	375	1409.1	220	420	3.301	4.988	899.8	428	761.4	254	429	1.344	1.382
J4	32306.2	377	58188.4	258	378	2.589	3.68	502.3	369	1223.2	252	427	2.750	4.798	1239.5	428	1221.7	254	429	1.734	2.175
J5	21566.1	378	37739.7	258	378	2.537	3.624	950.9	444	855.7	220	420	2.006	3.003	545.6	417	509.1	244	389	1.033	0.982
J6	57886.6	376	97589.7	258	378	3.423	5.393	735.5	381	2082.4	220	420	3.179	4.578	/	/	/	/	/	/	/
J7	67287.6	379	111268.0	258	378	3.291	5.057	1253.6	374	1054.2	254	379	2.629	3.830	/	/	/	/	/	/	/
J8	32193.6	376	54699.9	260	375	2.55	3.786	1970.0	439	1750.6	252	422	2.349	3.525	1926.1	429	1655.4	260	425	1.465	1.797
J9	63050.5	375	105888.8	258	378	3.156	4.992	2037.0	377	1680.8	258	373	2.545	3.664	/	/	/	/	/	/	/
J10	60074.3	376	103598.4	258	378	2.859	4.302	1648.2	377	1448.3	260	375	2.465	3.556	3305.6	414	2858.0	258	428	2.304	3.197
J11	53355.8	379	93181.8	258	378	2.805	4.336	1589.5	374	1313.9	258	373	2.514	3.566	/	/	/	/	/	/	/
J12	60774.8	375	101038.3	258	378	2.794	4.363	551.8	376	1776.5	220	420	2.768	4.242	2476.2	422	2134.9	258	428	2.079	2.699
J13	52569.1	376	83181.8	258	378	3.246	5.023	758.8	372	909.1	220	420	3.430	5.482	/	/	/	/	/	/	/
J14	70466.4	376	83181.8	258	378	3.246	5.023	454.8	386	1438.5	254	374	2.561	3.567	/	/	/	/	/	/	/

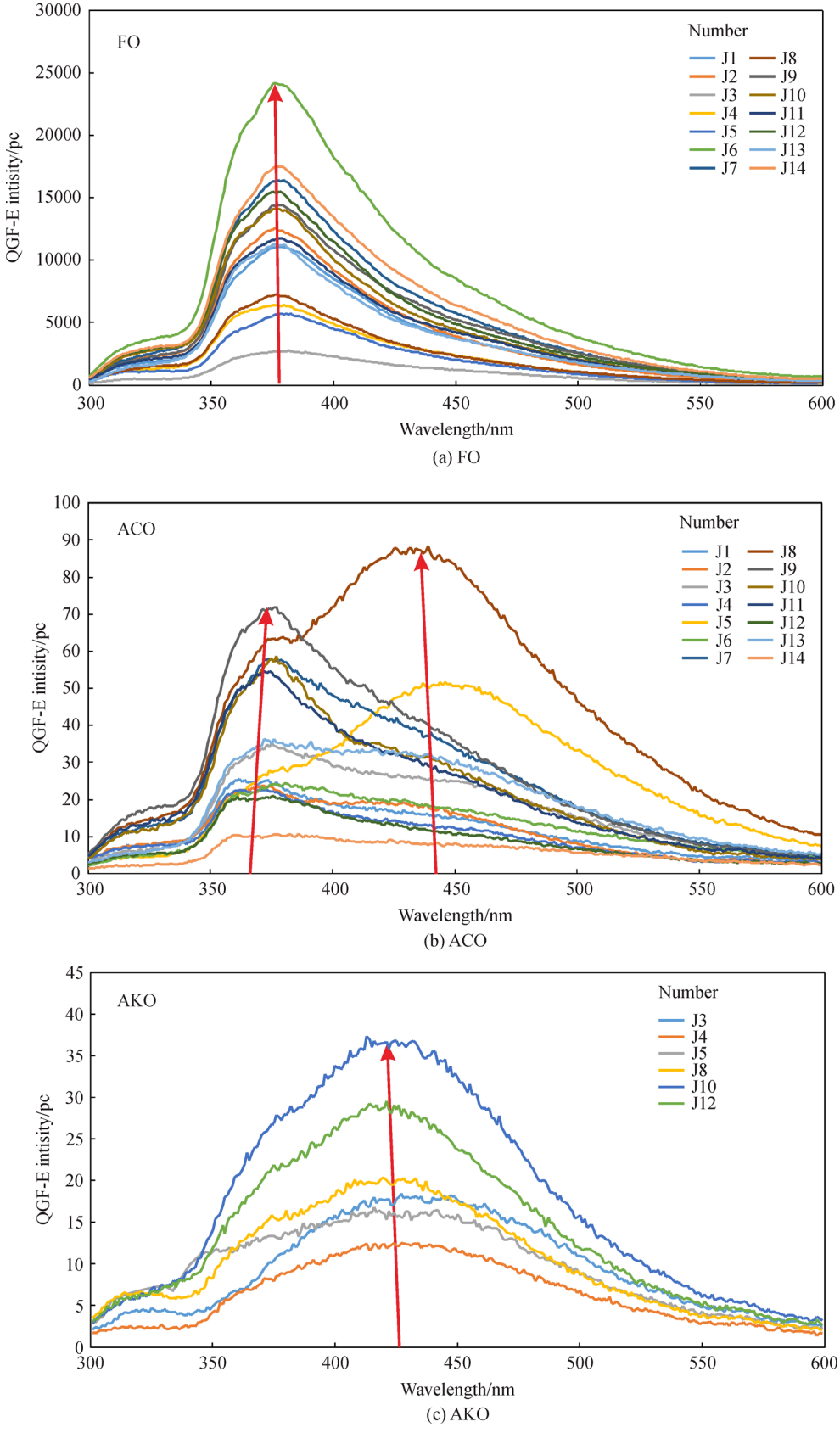

Fig. 7 QGF-E spectrum of shale oils in different phase states.

4.2.3 TSF of shale oils in different phase states

The normalized TSF Max of the FO samples ranges from 17722.7 pc to 111268 pc. The Max Ex of the FO samples is 258 nm and the Max Em ranges from 378 nm to 383 nm. The R_1 value is greater than 3. The normalized TSF Max of the ACO samples ranges from 467.6 pc to 2082.4 pc. The Max Ex ranges from 220 nm to 260 nm and Max Em ranges from 360 nm to 430 nm. R_1 values range from 1.5 to 3.5. The normalized TSF Max of the AKO samples ranges from 509.1 pc to 2858 pc. The Max Ex of the AKO samples ranges from 240 nm to 260 nm, and the Max Em ranges from 385 nm to 430 nm. As shown in Fig. 8, the TSF spectrum peaks of shale oils in different phase states are recorded at different wavelengths and amplitudes.

5 Discussion

5.1 Fluorescing source of the continental shale grain

As mentioned above, the soluble OM in the Q1 Formation is primarily composed of saturated and aromatic hydrocarbon compounds (Fig. 5), which is consistent with fact that the oil in the Q1 Formation is a medium heavy oil (Liu et al., 2019a). Additionally, the QGF intensity of shale grain shows a positive correlation to the content of non-hydrocarbons and asphaltenes (Fig. 9(a)), with a high determination coefficient (R^2 = 0.78). Shale grain QGF intensity shows a negative correlation to saturated and aromatic hydrocarbon content (Fig. 9(b)), with a determination coefficient (R^2 = 0.56). Carbonate-rich sample (J3, J5, J13) have abnormally high fluorescence intensity when compared to the other shale samples (Figs. 6(a) and 6(b)). The fluorescence spectra of the J3 and J5 samples show an obvious redshift with an emission wavelength greater than 370 nm (Fig. 6(a)), indicating that in these samples, the fluorescing organic compounds are more polar. The QGF spectra of the carbonate-rich samples excited by 228 nm light show minor changes when compared to those excited by 254 nm light (Fig. 6(b)). The QGF intensity of shale grain under 228 nm light shows a negative correlation with non-hydrocarbon and asphaltene content (Figs. 9(a) and 9 (b)). This indicates that non-hydrocarbons and asphaltenes on mineral grain surfaces are the main fluorescing sources excited during QGF detection.

As shown in Fig. 9(c), carbonate mineral content shows a positive correlation with the content of non-hydrocarbons and aromatic hydrocarbons, with a high coefficient of determination (R^2 = 0.67). By contrast, the carbonate mineral content shows a negative correlation to the content of saturated and aromatic hydrocarbon contents (Fig. 9(d)), with a coefficient of determination (R^2 = 0.54). The parameters; QGF intensity and QGF MAX, which represent hydrocarbon content were clearly reduced, indicating that a lot of the adsorbed hydrocarbons on the shale grain surfaces had been removed by ultrasonic vibration in DCM solution. It is clear however, that some of the adsorbed hydrocarbons remain on the shale grain surfaces. The carbonate-rich samples still show abnormally high fluorescence intensities following ultrasonic vibration (Table 3), with the fluorescence spectrum peaks λ_{max} of the J3 and J5 samples at 517.6 nm and 528.8 nm, respectively. As mentioned before, non-hydrocarbons and asphaltenes are the main fluorescing source observed during the QGF experiments. This suggests that non-hydrocarbons and asphaltenes accumulate on the surfaces of carbonate minerals, resulting in abnormally high fluorescence intensities recorded during the QGF experiment. Using an excitation wavelength of 228 nm does not eliminate the abnormally high fluorescence intensities recorded from samples with high carbonate mineral content. Due to the large surface area of clay crystals, when compared to carbonate minerals, clay minerals are generally considered to be more favorable candidates for the retention of high polarity, non-hydrocarbon and asphaltene compounds. However, the QGF results from the Q1 Formation shales show that the carbonate grain surfaces are favorable for the enrichment of non-hydrocarbon and asphaltene compounds. It is clear that a fraction of non-hydrocarbon and asphaltene compounds cannot be extracted by the process of ultrasonic vibration. During the OM maturation process, the adsorption of non-hydrocarbon and asphaltene compounds onto the surface of carbonate minerals is commonplace, with some non-hydrocarbons and asphaltenes combining with carbonate minerals via chemical bonding (Liu et al., 2019c).

In general, non-hydrocarbons and asphaltenes are the main contributors to the fluorescence intensity recorded during QGF detection. It is easy for non-hydrocarbons and asphaltene components to become adsorbed onto the surface of carbonate minerals during hydrocarbon generation and expulsion, resulting in abnormally high recorded QGF intensities. It should however be noted that shale reservoirs showing strong QGF intensities should not generally be considered as “sweet spots” for the enrichment of saturated hydrocarbons and aromatic hydrocarbons. Decreasing the excitation wavelength to 228 nm for the carbonate-rich samples did not eliminate misleading anomalously high measured QGF intensities. Therefore, QGF applied to continental shale grain will not result in the identification of a shale interval rich in hydrocarbons and may instead mislead investigators.

It should be noted that in this study there was a lack of samples with carbonate mineral content ranging between 15% and 80%, and furthermore, the question of whether different species of carbonate minerals would affect the oils in different phase states remains to be resolved. Future investigations will be designed to address these issues.

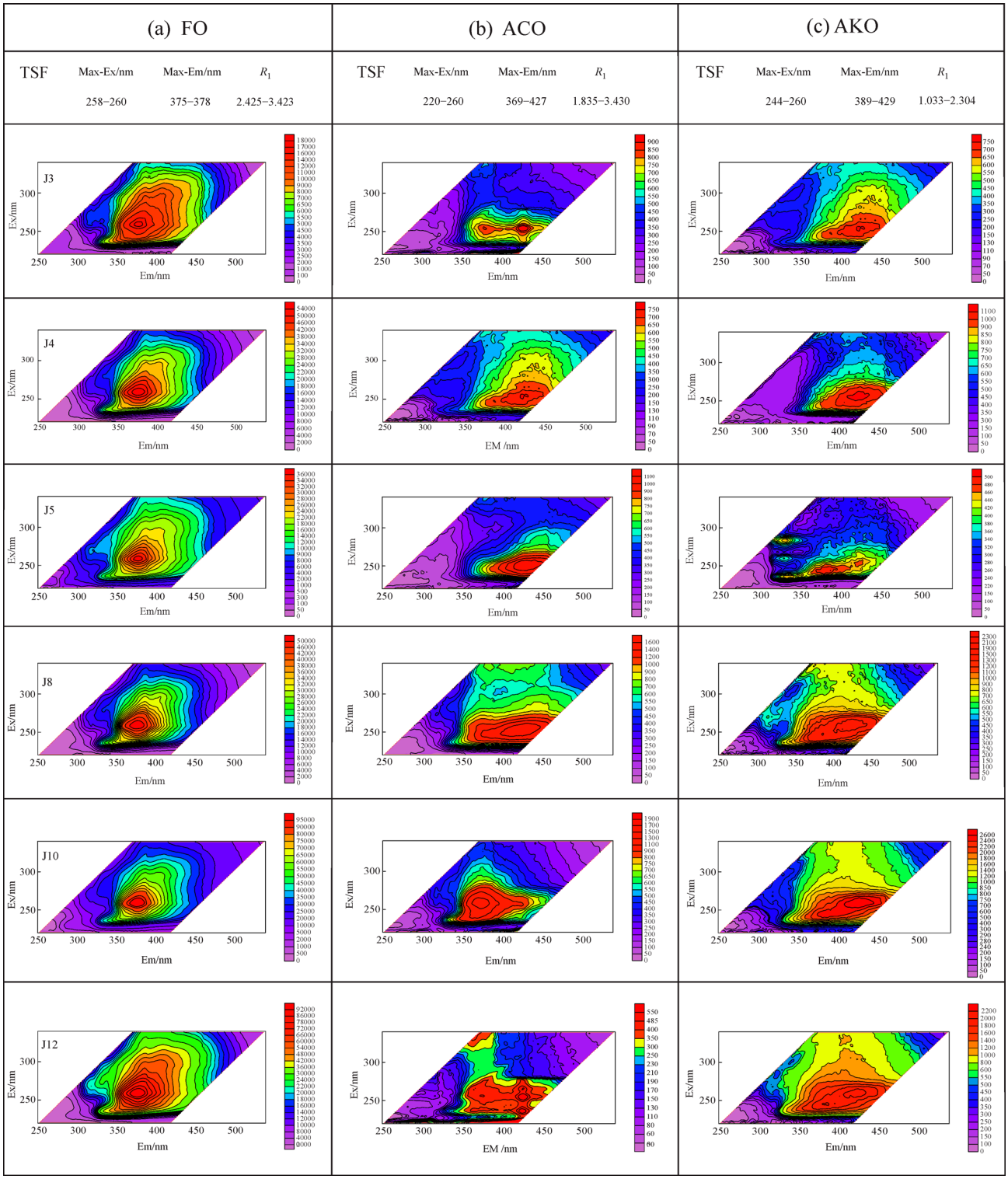

Fig. 8 TSF spectrum of shale oils in different phase states.

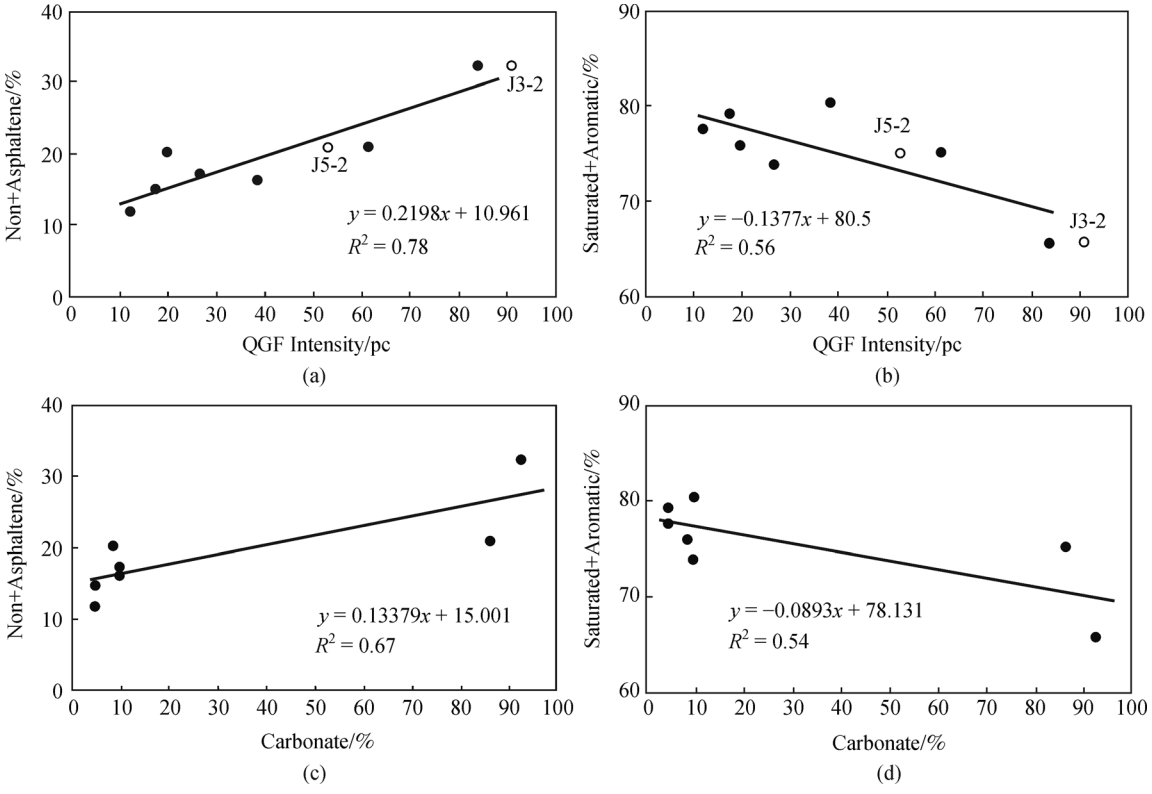

Fig. 9 (a) Correlation between QGF intensity and the sum of non-hydrocarbon and asphaltene. (b) Correlation between QGF intensity and the sum of saturated and aromatic hydrocarbon. (c) Correlation between Carbonate minerals content and the sum of non-hydrocarbon and asphaltene. (d) Correlation between Carbonate minerals content and the sum of saturated and aromatic hydrocarbon.

5.2 Relationships between recorded fluorescence spectra and oil in different phase states

Positive correlations were observed between normalized FO QGF-E intensity, EOM content and S_1, (Fig. 10(a)). An excellent positive correlation between normalized FO QGF-E intensity and FO TSF intensity was also observed (Fig. 10(b)), with a high coefficient of determination (R^2 = 0.99). As mentioned before, the parameter S_1 represents most of the relatively light hydrocarbons in shale samples, while EOM represents the total oil content of the shale reservoirs. The observation that normalized FO QGF-E intensity correlates well with both of these parameters means that both QGF-E and TSF can be used to delineate the free oil content in a shale reservoir. When combined with TSF detection of crude oil from the Q1 Formation, total oil saturation can be quantified (Liu et al., 2019b).

There is no obvious correlation between the normalized ACO QGF-E intensity and the content of carbonate minerals (Fig. 10(c)). The detection of minerals is semiquantitative, and the error in this value is further increased owing to the low carbonate content in the samples used during the fluorescence experiments. Additionally, due to the complex mineral composition of continental shales, hydrochloric acid treatment leads to the dissolution of other easily eroded minerals in the shale samples, and hydrocarbon compounds that are removed along with these easily eroded minerals will also affect the experimental results. No obvious correlation between the normalized ACO QGF-E intensity and TOC were observed (Fig. 10(d)), indicating that the ACO content is not solely controlled by OM content in this study.

A positive correlation between normalized AKO QGF-E intensity and TOC was observed (Fig. 10(e)), with a high coefficient of determination (R^2 = 0.91), indicating that AKO is the primary contributor to adsorbed hydrocarbons on OM surfaces, meaning AKO content is controlled by OM abundance.

It should be noted that in the study of conventional sandstone reservoirs (Liu and Eadington, 2005), a reservoir sand is considered to be an oil reservoir when the normalized FO QGF-E intensity exceeds 40 pc. In this study, the normalized FO QGF-E intensity ranges from 9893.6 pc to 70466.4 pc. This means that if the normalized FO fluorescence intensity of is used to identify oil-rich shale intervals, a cut-off value needs to be separately defined. The TSF R_1 parameter can be used to reflect the ratio of tricyclic and monocyclic aromatics in oil, and as such can be used as an oil maturity index (Reyes, 1994; Barwise and Hay, 1996). Furthermore, there is a negative

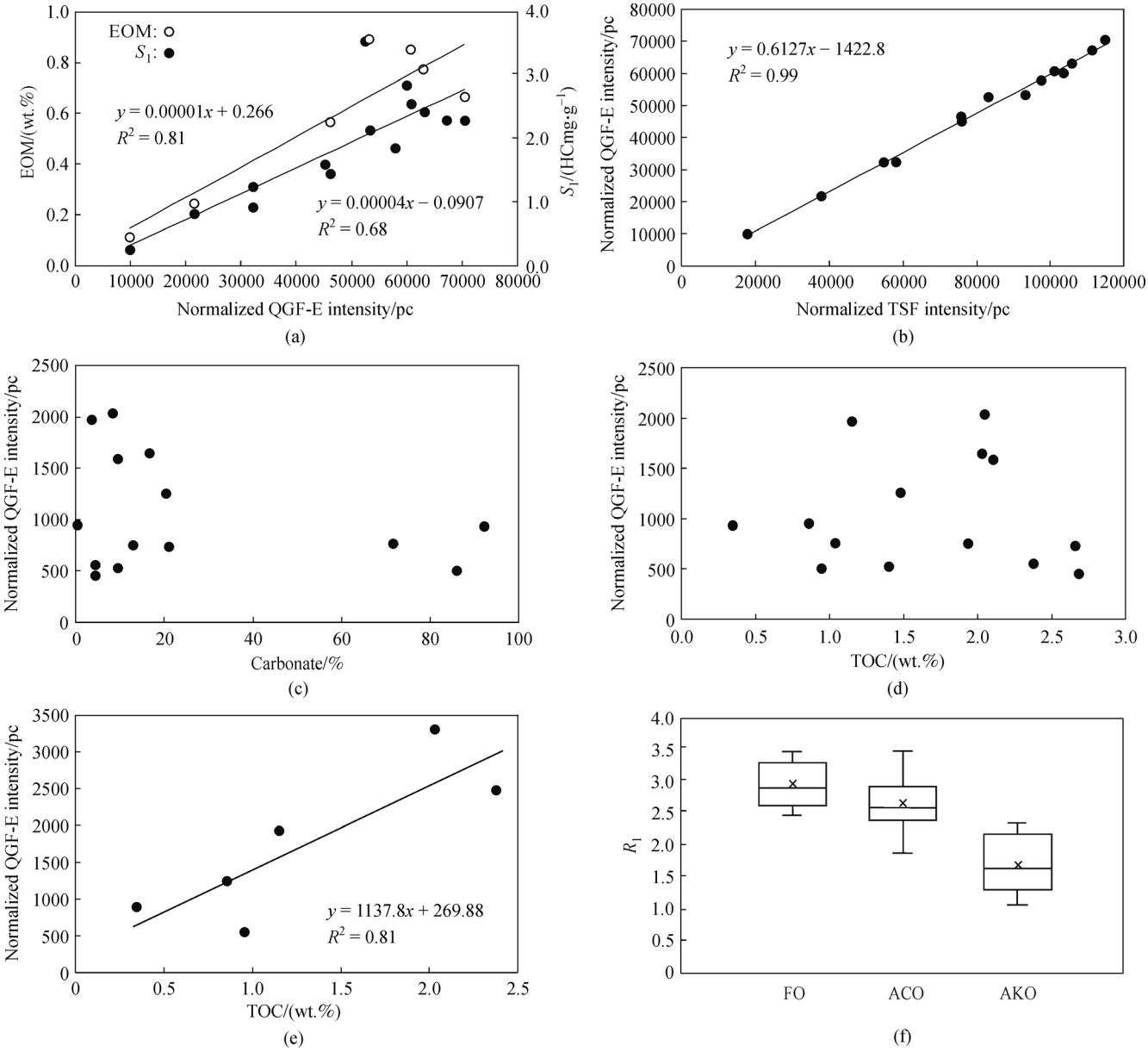

Fig. 10 (a) Correlations between the normalized FO QGF-E intensity and S_1, EOM respectively. (b) Correlation between the normalized FO QGF-E intensity and normalized TSF intensity of FO. (c) Correlation between the normalized ACO QGF-E intensity and Carbonate minerals. (d) Correlation between the normalized ACO QGF-E intensity and TOC. (e) Correlation between the normalized AKO QGF-E intensity and TOC. (f) TSF R_1 distribution of shale oil in different phase states.

correlation between TSF R_1 and biomarkers of TS and TM, which again could be used to indicate crude oil maturity (Liu et al., 2014a). The higher the R_1 value is, the lower the crude oil maturity, and the more viscous the oil. In some studies of hydrocarbons trapped in inclusions, this correlation breaks down due to the OM source and the sedimentary environment (Moldowan et al., 1986; Radke et al., 1998). In this study, the measured TSF R_1 value for FO is the highest, followed by ACO and AKO values (Fig. 10(f)). The value of R_1 only indicates that the ratio of tricyclic aromatic hydrocarbons in FO is high.

5.3 Compositional differences of shale oils in different phase states relating to the oil generation period

The characteristics of the fluorescence spectra of shale oils in different phase states show clear differences. The fluorescence spectrum peaks λ_{max} of FO are seen at around 380 nm (Fig. 11(a)), and a single hump distribution skewed to the left side of the spectrum indicates that FO composition is relatively uniform. The fluorescence spectrum characteristics of most ACO samples are similar to that of FO, and the fluorescence spectrum peaks λ_{max} are

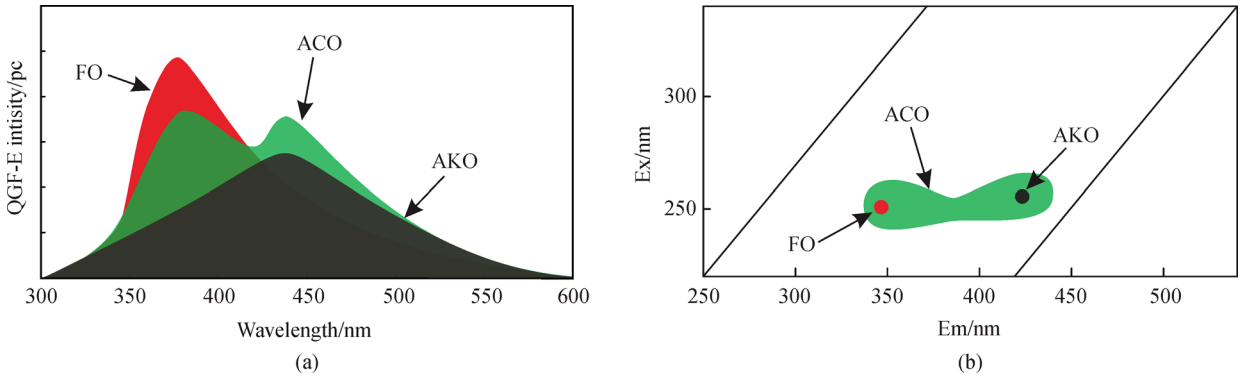

Fig. 11 (a) Cross plot of QGF-E spectrum of shale oils in different phase states. (b) Cross plot of TSF spectrum of shale oils in different phase states.

also around 380 nm. The fluorescence spectrum peaks λ_{max} of samples J5 and J8 are seen at 400 nm as the fluorescence spectra red-shifts. The fluorescence spectrum of AKO shows clear differences with those of the FO and ACO. The AKO fluorescence spectrum peaks λ_{max} are at around 400 nm. From FO to ACO, AKO, under the same excitation wavelength, the fluorescence wavelength increases continuously, showing a redshift in the fluorescence spectra. Furthermore, on the TSF spectra of oil in different phase states (Fig. 11(b)), FO only shows a single characteristic hump, skewed to the left side. In addition to the characteristic left humped distribution similar to FO, the ACO samples from J3 and J13 also show a humped distribution skewed to the right. In these samples, the TSF spectrum is shifted to the right relative to FO, the average value of Max Em is 401 nm and the average value of Max Ex is 240 nm. The TSF spectrum of AKO shows a single distribution with a characteristic peak skewed to the right. The average value of Max Em is 421 nm and the average value of Max Ex is 255 nm. The fluorescence spectrum of polar compounds shows a redshift when compared to saturated hydrocarbons and aromatic hydrocarbons, which indicates extensive condensation of aromatic structures and a lack of saturates (Khorasani, 1986). The gradual redshift observed in the fluorescence spectrum from FO to ACO and to AKO indicates that the hydrocarbon components in different oil phase states are becoming progressively heavier. FO is primarily composed of relatively light hydrocarbon compounds, and the aromatization of the hydrocarbon compounds in ACO and AKO increases gradually. AKO contains the largest amount of polar compounds. Furthermore, if the parameter TSF R_1 is a solid index of the maturity of crude oil in this study, the values obtained for this parameter from the FO samples would indicate that the maturity and polar compound content of FO is the highest of the three phase states (Fig. 10(f)). Clearly this is inconsistent with the TSF and QGF-E spectrum characteristics from the oil in different phase states. The TSF R_1 values obtained indicate simply that the ratio of tricyclic aromatic hydrocarbons to monocyclic aromatic hydrocarbons in FO is high. In this study area, the TSF R_1 parameter is not a reliable indicator of oil maturity.

The organic matter in the mature Q1 Formation shales is primarily type I and type IIa kerogens with good homogeneity (Figs. 4(a) and 4(b)). It should follow that the hydrocarbon compounds of shale oils in different phase states should have relatively consistent compositions, however the fluorescence investigations clearly show different hydrocarbon compounds present in each of the three phase states. This suggests that during maturation of the OM, followed by hydrocarbon generation and expulsion from the shale reservoirs, the hydrocarbon compounds with different polarities and compositions underwent fractionation, which led to the observed differences in oil content and hydrocarbon composition of the shale oils in different phase states.

6 Conclusions

During the fluorescence experiments, the abnormally strong QGF intensity measured from carbonate-rich shale grain samples could be caused by non-hydrocarbons rather than hydrocarbons, this will affect the identification of shale intervals rich in hydrocarbons. The normalized QGF-E and TSF intensities have positive correlations with oil content, making them effective indexes for the evaluation of shale oil content.

The oil phase states of the Q1 Formation are dominated by FO, of which the QGF-E normalized fluoresce intensity (with an average value of 48059 pc) is 2–3 orders of magnitude larger than that of other oil phases (with an average value of 1252 pc). The content of AKO is controlled by the original OM content.

The hydrocarbon compositions of shale oils in various phase states in the Q1 Formation are quite different. This is the result of fractionation of hydrocarbon components that occurs during the maturation of OM and subsequent

hydrocarbon generation and expulsion. FO contains the lightest hydrocarbons, followed by ACO, AKO contains the heaviest hydrocarbon components.

Acknowledgements This study is funded by the National Natural Science Foundation of China (Grant No.41972156) and the Science and Technology Project of Heilongjiang Province (No.2020ZX05A01).

References

Barwise T, Hay S (1996). Predicting oil properties from core fluorescence. In: Schumacher D, Abrams M A, eds. Hydrocarbon Migration and Its Near Surface Expression. American Association of Petroleum Geologists Memoir, 66: 363–371

Curtis J B (2002). Fractured shale-gas systems. AAPG Bull, 86: 1921–1938

Espitalié J, Marquis F, Barsony I (1984). Geochemical logging. In: Voorhess K J, ed. Analytical Pyrolysis. Boston: Butterworths: 53–79

Fleury M, Romero-Sarmiento M (2016). Characterization of shales using T1–T2 NMR maps. J Petrol Sci Eng, 137: 55–62

Gao Z, Fan Y, Xuan Q, Zheng G (2020). A review of shale pore structure evolution characteristics with increasing thermal maturities. Adv Geo-Energy Res, 4(3): 247–259

Gong L, Wang J, Gao S, Fu X, Liu B, Miao F, Zhou X, Meng Q (2021). Characterization, controlling factors and evolution of fracture effectiveness in shale oil reservoirs. J Petrol Sci Eng, 203: 108655

Guan P, Xu Y, Liu W (1998). Quantitative estimates of different existing state organic matter in source rocks. Chin Sci Bull, 43: 1556–1559 (in Chinese)

Guo X, Huang Z, Ding X, Chen J, Chen X, Wang R (2018). Characterization of continental coal-bearing shale and shale gas potential in Taibei sag of the Turpan Hami Basin, NW China. Energy Fuels, 32(9): 9055–9069

Hou Y, Wang F, He S, Dong T, Wu S (2017). Properties and shale oil potential of saline lacustrine shales in the Qianjiang Depression, Jianghan Basin, China. Mar Pet Geol, 86: 1173–1190

Jarvie D M (2012). Shale resource systems for oil and gas: Part 2-shale-oil resource systems. In: Breyer J A, ed. Shale Resevoirs—Giant Resources for the 21st Century: AAPG Memoir 97, 89–119

Jarvie D M, Hill R J, Ruble T E, Pollastro R M (2007). Unconventional shale-gas systems: the Mississippian Barnett shale of north-central Texas as one model for thermogenic shale-gas assessment. AAPG Bull, 91(4): 475–499

Jiang Q, Li M, Qian M, Li Z, Li Z, Huang Z, Zhang C, Ma Y (2016). Quantitative characterization of shale oil in different occurrence states and its application. Petrol Geol & Exper, 38: 842–849 doi: 10.11781/sysydz201606842 (in Chinese)

Khorasani G K (1986). Novel development in fluorescence microscopy of complex organic mixtures: application in petroleum geochemistry. Organic Geochem, 11(3): 157–168

Langford F F, Blanc-Valleron M M (1990). Interpreting Rock-Eval pyrolysis data using graphs of pyrolizable hydrocarbons vs. total organic carbon. Am Assoc Pet Geol Bull, 74: 799–804

Li J, Jiang C, Wang M, Lu S, Chen Z, Chen G, Li J, Li Z, Lu S (2020). Adsorbed and free hydrocarbons in unconventional shale reservoir: a new insight from NMR T1–T2 maps. Mar Pet Geol, 116: 104311

Li M, Chen Z, Ma X, Cao T, Li Z, Jiang Q (2018). A numerical method for calculating total oil yield using a single routine Rock-Eval program: a case study of the Eocene Shahejie Formation in Dongying Depression, Bohai Bay Basin, China. Int J Coal Geol, 191: 49–65

Li M, Chen Z, Ma X, Cao T, Qian M, Jiang Q, Tao G, Li Z, Song G (2019). Shale oil resource potential and oil mobility characteristics of the Eocene-Oligocene Shahejie Formation, Jiyang Super-Depression, Bohai Bay Basin of China. Int J Coal Geol, 204: 130–143

Li T, Huang Z, Feng Y, Cheng X, Ma Q, Liu B, Guo X (2020). Reservoir characteristics and evaluation of fluid mobility in organic-rich mixed siliciclastic-carbonate sediments: a case study of the lacustrine Qiketai Formation in Shengbei Sag, Turpan-Hami Basin, northwest China. J Petrol Sci Eng, 185: 106667

Li Z, Zou Y R, Xu X, Sun J, Li M, Peng P (2016). Adsorption of mudstone source rock for shale oil–Experiments, model and a case study. Org Geochem, 92: 55–62

Liu B, Bai L, Chi Y, Jia R, Fu X, Yang L (2019a). Geochemical characterization and quantitative evaluation of shale oil reservoir by two-dimensional nuclear magnetic resonance and quantitative grain fluorescence on extraction: a case study from the Qingshankou Formation in Southern Songliao Basin, northeast China. Mar Pet Geol, 109: 561–573

Liu B, He J, Lü Y, Ran Q, Dai C, Li M (2014a). Parameters and method for shale oil assessment: taking Qingshankou Formation shale oil of northern Songliao Basin. J Cent South Univ (Science and Technology), 45: 3846–3852 (in Chinese)

Liu B, Sun J, Zhang Y, He J, Fu X, Yang L, Xing J, Zhao X (2021). Reservoir space and enrichment model of shale oil in the first member of Cretaceous Qingshankou Formation in the Changling sag, southern Songliao Basin, NE China. Pet Explor Dev, 48(3): 608–624

Liu B, Wang H, Fu X, Bai Y, Bai L, Jia M, He B (2019b). Lithofacies and depositional setting of a highly prospective lacustrine shale oil succession from the Upper Cretaceous Qingshankou Formation in the Gulong sag, northern Songliao Basin, northeast China. AAPG Bull, 103(2): 405–432

Liu B, Yang Y, Li J, Chi Y, Li J, Fu X (2020). Stress sensitivity of tight reservoirs and its effect on oil saturation: a case study of Lower Cretaceous tight clastic reservoirs in the Hailar Basin, Northeast China. J Petrol Sci Eng, 184: 106484

Liu C L, Wang Z, Guo Z, Hong W, Dun C, Zhang X, Li B, Wu L (2017). Enrichment and distribution of shale oil in the Cretaceous Qingshankou Formation, Songliao Basin, northeast China. Mar Pet Geol, 86: 751–770

Liu K, Eadington P (2005). Quantitative fluorescence techniques for detecting residual oils and reconstructing hydrocarbon charge history. Org Geochem, 36(7): 1023–1036

Liu K, Eadington P, Middleton H, FentonS, Cable T (2007). Application of quantitative grain fluorescence techniques in investigating hydrocarbon charge history in some major petroleum producing basins in Australia and Papua New Guinea. J Petrol Sci Eng, 57: 139–151

Liu K, George S C, Eadington P J (2003). Predicting abundances and n-alkane profiles of oil inclusions from bulk fluorescence spectroscopy.

In: 21st International Meeting on Organic Geochemistry. Book of Abstracts Part II. EAOG, Kraków, 177–178

Liu K, George S C, Lu X, Gong S, Tian H, Gui L (2014b). Innovative fluorescence spectroscopic techniques for rapidly characterising oil inclusions. Org Geochem, 72: 34–45

Liu K, Ostadhassan M (2019). The impact of pore size distribution data presentation format on pore structure interpretation of shales. Adv Geo-Energy Res, 3(2): 187–197

Liu K, Xiao X, Mills D, George S C, Volk H, Gong S (2009). Cautions in the interpretation of petroleum fluid inclusion data in petroleum system analysis: insight from spectroscopic analyses of naturally occurred and synthetic petroleum inclusions. J Geochem Explor, 101: 62

Liu P, Wang X, Li X, Zhang T, Liu W (2019c). Geochemical characteristics of released organic matters by acid decomposition of hydrocarbon source rocks from different sedimentary basins. Geofluids, 2019: 4816218

Loucks R G, Reed R M, Ruppel S C, Hammes U (2012). Spectrum of pore types and networks in mudrocks and a descriptive classification for matrix-related mudrock pores. AAPG Bull, 96(6): 1071–1098

Moldowan J M, Sundararaman P, Schoell M (1986). Sensitivity of biomarker properties to depositional environment and/or source input in the Lower Toarcian of SW-Germany. Org Geochem, 10(4-6): 915–926

Morad S, Ketzer J M, De Ros L F (2000). Spatial and temporal distribution of diagenetic alterations in siliciclastic rocks: implications for mass transfer in sedimentary basins. Sedimentology, 47: 95–120

Pan Y, Li M, Sun Y, Li Z, Jiang Q, Liao Y (2018). Geochemical characterization of soluble organic matters with different existing states in low-maturity argillaceous source rocks of lacustrine facies. Geochimica, 47: 335–344 (in Chinese)

Pan Y, Li M, Sun Y, Li Z, Liu P, Jiang B, Liao Y (2019). Characterization of free and bound bitumen fractions in a thermal maturation shale sequence. Part 1: acidic and neutral compounds by negative-ion ESI FT-ICR MS. Org Geochem, 134: 1–15

Radke M, Hilkert A, Rullkötter J (1998). Molecular stable carbon isotope compositions of alkylphenanthrenes in coals and marine shales related to source and maturity. Org Geochem, 28(12): 785–795

Reyes M V (1994). Application of fluorescence techniques for mud-logging analysis of oil drilled with oil-based muds. SPE Form Eval, 9 (04): 300–305

Rivard C, Lavoie D, Lefebvre R, Sejourne S, Lamontagne C, Duchesne M (2014). An overview of Canadian shale gas production and environmental concerns. Int J Coal Geol, 126: 64–76

Romero-Sarmiento M F (2019). A quick analytical approach to estimate both free versus sorbed hydrocarbon contents in liquid rich source rocks. AAPG Bull, 103(9): 9

Romero-Sarmiento M F, Pillot D, Letort G, Lamoureux-Var V, Beaumont V, Huc A-Y, Garcia B (2015). New rock-eval method for characterization of unconventional shale resource systems. Oil & Gas Sci Tech, 71: 37

Spiro B (1978). Thermal effects in “oil shales”, naturally occurring kaolinite and metakaolinite organic associations. Chem Geol, 25(1–2): 67–78

Spiro B (1984). Effects of mineral matrix on the distribution of geochemical markers in thermally affected sedimentary sequences. Org Geochem, 6: 543–559

Stasiuk L D, Snowdon L R (1997). Fluorescence micro-spectrometry of synthetic and natural hydrocarbon fluid inclusions: crude oil chemistry, density and application to petroleum migration. Appl Geochem, 12: 229–241

Sun L, Liu H, He W, Li G, Zhang S, Zhu R (2021). An analysis inof major scientific problems and research paths of Gulong shale oil in Daqing Oilfield, NE China. Pet Explor Dev, 48(3): 453–463

Zeng F, Dong C, Lin C, Wu Y, Tian S, Zhang X, Lin J (2021). Analyzing the effects of multi-scale pore systems on reservoir properties—a case study on Xihu Depression, East China Sea Shelf Basin, China. J Petrol Sci Eng, 203: 108609

Zhang H, Huang H, Li Z, Liu M (2019). Oil physical status in lacustrine shale reservoir–a case study on Eocene Shale Formation shales, Donging Depression, East China. Fuel, 257: 116027

Zou C, Dong D, Wang S, Li J, Li X, Wang Y, Li D, Cheng K (2010). Geological characteristics, formation mechanism and resource potential of shale gas in China. Pet Explor Dev, 37: 641–653